THE STRUCTURAL DESIGN OF TALL AND SPECIAL BUILDINGS
Struct. Design Tall Spec. Build. 2016;
Published online in Wiley Online Library (wileyonlinelibrary.com/journal/tal). DOI: 10.1002/tal.1306

Seismic assessment of RC core-wall building capable of three plastic hinges with outrigger

Hamid Beiraghi[1]* and Navid Siahpolo[2]

[1]*Department of Civil Engineering, Mahdishahr Branch, Islamic Azad University, Mahdishahr, Iran*
[2]*Department of Civil Engineering, ACECR Institute for Higher Education, Khuzestan Iran*

SUMMARY

In a core-wall structure with buckling restrained braces (BRB) outrigger, locations of the plastic hinges are influenced by the outrigger action. Therefore, the designer should consider the issue and use suitable details in the plastic hinge area. The essential questions that arise here are the plastic hinge location and the design moment demand used for design of this kind of structure. In this paper, responses of the core-wall buildings with BRB outrigger designed by using the traditional response spectrum analysis procedure are assessed by implementing the nonlinear time history analysis. The result demonstrates that the plasticity can extend over anywhere within the core-walls specially, at the base and above or below the outrigger levels. Formation of three plastic hinges in the core-wall is recognized suitable for the system. To control the plasticity extension in the core-wall, it is recommended that a new modal combination method be applied to calculate the moment strength of the three plastic hinges over the height. A capacity design concept is used to design other regions of the core-wall where the plasticity does not extend to. The proposed procedure improves behavior of the system by restricting the plasticity extension to the predefined plastic hinge regions. Copyright © 2016 John Wiley & Sons, Ltd.

Received 15 January 2016; Revised 12 May 2016; Accepted 30 June 2016

KEY WORDS: reinforced concrete; core-wall; plastic hinge; BRB; outrigger; NLTHA

1. INTRODUCTION

In tall buildings, controlling structural deformation subjected to the lateral load is a challenging issue (Chen *et al*., 2010; Satake *et al*., 2003; Smith and Coull, 1991; Smith and Willford, 2007; Soong and Spencer, 2002). Commonly, 35 to 40-story buildings do rely solely on the core-wall systems. The lateral resistance of these systems against displacement decreases severely for the taller buildings (Rahgozar and Sharifi, 2009; Xu *et al*., 1999). Using outrigger system, the lateral stiffness increases up to 25 to 30 % compared with a system lacking such trusses (Taranath, 1988). Taranath studied the optimum location of a single outrigger in the structural system with the aim of reducing roof drift subjected to the wind load and presented an approximate method of analysis. In a single-outrigger system with rigid outrigger and subjected to the uniform-distributed lateral load, the optimum location is obtained approximately at 0.5H, where H is the total height of the building (Taranath, 1974). Outrigger system under triangular load has been studied, and the results showed that the optimum location of the outriggers under triangular lateral load was slightly higher than those deduced for uniformly distributed loading (Smith and Salim, 1981; Wu and Li, 2003).

The behavior of viscous damper under moderate earthquakes is roughly equal to that of the bare structures. However, by increasing the earthquake intensity, the influence of viscous damper becomes more obvious (Zhou and Li, 2013).

*Correspondence to: Hamid Beiraghi, Department of Civil Engineering, Mahdishahr Branch, Islamic Azad University, Mahdishahr, Iran.
E-mail: H_beiraghi@yahoo.com

Generally, buckling restrained braced frame is a diagonally braced frame employing buckling restrained braces that is a kind of concentrically braced frame. Provisions for the design of such systems are not available in the codes of some countries (Bosco and Marino, 2013). Codes such as AISC 2010, Seismic Provision for Structural Steel Buildings, represent response modification factor and intend to ensure that braces remain within their range of deformation capacity, and yielding of the other columns and beams is restricted (AISC, 2010). Some codes, such as EC8, do not present response modification factor or provision regarding the use of capacity design principles to be applied on the beam and column members in the buckling restrained braced frames (CEN EC8, 2004). AISC 2010 requires that values of the response modification factor be equal to either 7 or 8 in the case of pinned or moment-resistant beam-to-column connections in the frames, respectively. Some researches emphasized that the response modification factor decreases as the height of the structure increases (Asgarian and Shokrgozar, 2009; Kim *et al*., 2009; Mahmoudi and Zaree, 2010)

Reinforced concrete (RC) core-wall is an interesting structural system used in tall buildings (Klemencic *et al*., 2007). Design codes allow the extension of plasticity in limited regions of the structural system during severe ground motions. In the case of cantilever RC walls, formation of the plastic hinge should preferably be located at the base region of the wall (CEN EC8, 2004; CSA Standard A23.3-04, 2005; NZS 3101, 2006).

In the response spectrum analysis (RSA) procedure, the elastic responses of each vibration mode determined using the design-based earthquake (DBE) with 5% damping response spectrum are reduced by a response modification factor (or reduction factor), R, in order to calculate the desired design level demands. Commonly, in the RSA procedure, modal responses are reduced by an identical R factor for all modes. Several researchers have demonstrated that the formation of plastic hinges at the base of the cantilever walls essentially reduces response of the first vibration mode, while higher vibration modes are not reduced to the same degree as the first mode (Beiraghi *et al*., 2016a). Therefore, the conventional RSA procedure is not an appropriate approach for designing of cantilever walls with plasticity at the base (Priestley *et al*., 2007). Panagiotou *et al*. proposed an approach for the RC core-wall building that considers only the first two response modes with different response modification factors for each of them (Calugaru and Panagiotou, 2012). Besides, dual plastic hinge approach was investigated for the cantilever core-wall buildings. In this approach, one plastic hinge at the wall base and another at the mid height were allowed. In this approach, more energy dissipation and less moment demand occur during a strong earthquake (Panagiotou and Restrepo, 2009). Besides, Beiraghi *et al*. studied responses of RC core-wall structures with multiplastic hinges (Beiraghi *et al*., 2016a,b).

Nonlinear seismic responses of the core-wall structures containing buckling restrained braces (BRB) outrigger subjected to earthquake vibrations have not yet been investigated enough. BRB outriggers can change the force distribution and deformation demand quantity of the core-walls over the height and lead to the new plastic hinge arrangement over the core-wall height. In this paper, the outrigger–core-wall buildings are designed using the traditional RSA. Then, the nonlinear time history analysis of the system is carried out, and the responses are investigated. It is demonstrated that in the conventional approach, plasticity could extend anywhere in the core-wall, especially above the outrigger level. Because of variation of the moment diagram due to the outrigger action, formation of three plastic hinges in the core-wall is preferable for the core-wall structure. A new modal combination method is proposed for flexural design of the three plastic hinges, and a capacity design concept is used for the flexural design of other regions. The results show that the new approach leads to the desirable responses.

2. CONVENTIONAL DESIGN PROCEDURE

In this study, the responses of 40-story, 50-story and 60-story outrigger buildings are examined. First, for the 40-story building, the outrigger is placed at 0.5H, 0.73H and at the highest level. Linear design of all the structures is accomplished by RSA procedure at DBE level using the spectrum displayed in Figure 1. ETABS software version 13.1.1 was implemented to design the structures (ETABS, Version 13.1.1, 2013). A response modification factor equal to 5 is used as recommended by the National Earthquake Hazards Reduction Program (NEHRP) Seismic Design Technical Brief No. 6 (National

DOI: 10.1002/tal

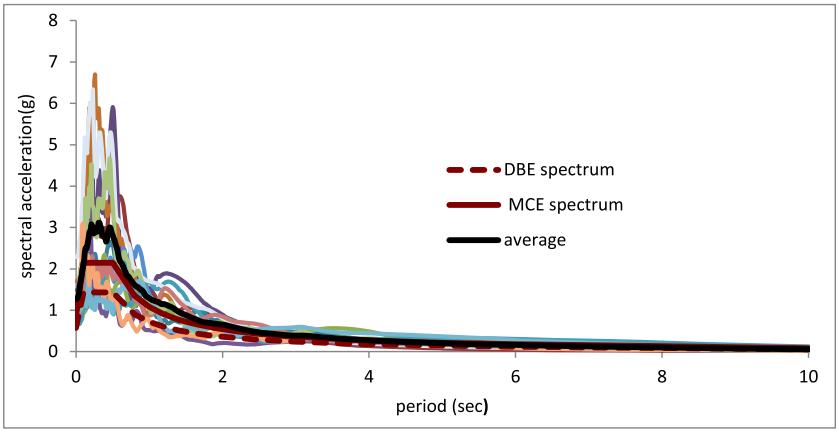

Figure 1. Response spectrum of the records and the target spectrum.

Institute of Standards and Technology, 2012). The lateral design forces were scaled to 85% of the base shear, calculated according to the equivalent static base shear procedure. The plan of the building and elevation view of the models are presented in Figure 2. The peripheral columns are of steel material. The model consists of core-wall, BRBs, beams in the plane of the outrigger and outside columns that are connected to the outriggers. The connection of the beams to the columns and connection of the BRBs to the other elements are pin type, and the connection of the core-wall to the base is fixed type.

2.1. Core-wall design

Shell-type elements are used to model the RC wall in ETABS. This type of element uses a triangular or quadrilateral formulation that combines the separate membrane and plate-bending behaviors. There are six deformation components for the element nodes. The RC core-wall, outrigger and connected outside columns carried all the earthquake lateral loads applied to the building. The distributed dead and live

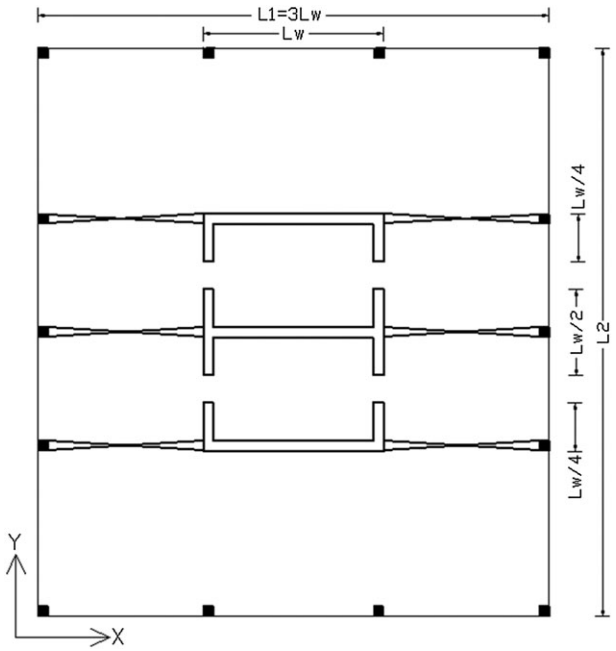

Figure 2. Plane of the structure and the outriggers.

DOI: 10.1002/tal

loads of the floors were 7 and 2 $\frac{KN}{m^2}$ respectively. The corresponding dead and live loads were carried by the core-wall, and the outside columns were assigned to them. The mass of each story was assigned to the center of mass of floors in the models. Design of the models was carried out based on the ASCE 7, ACI 318-11 and AISC 2010 codes (ACI 318-11, 2011; AISC, 2010; ASCE/SEI 7-2010, 2010). To account for the concrete cracks, a reduction factor equal to 0.5 was applied. This reduction factor was multiplied by the moment of inertia of the core-wall cross section, and its value is in accordance with the stiffness reduction factors recommended in the ACI 318-11 (Sections 8.8 and 10.10).

The nominal yielding strength of the steel reinforcement and the nominal compression strength of the concrete were 400 and 45 MPa, respectively. The yielding strength of the column steel was 370 MPa. Approximately, more than 96% of the modal participating mass ratio results from the first four translational vibration modes in the X direction. It should be noted that all the analyses and designs were limited to the X direction. In the core-wall, the minimum longitudinal reinforcement ratio was 0.25% (ACI 318-11, 2011). The boundary element length was in accordance with the ACI 318 and was extended to 10, 7 and 3% of the wall height from the base for the 40-story, 50-story and 60-story buildings, respectively. For all assumed models, the ratio of total height to the L1 was 4.67 (Figure 2). Elevation view of the designed models is shown in Figure 3.

2.2. Buckling restrained brace design

Design of the BRBs was conforming to the current prescriptive codes. To design the BRB braces, axial forces calculated from the modal RSA were reduced by an assigned value of the response modification factor. The capacity of the braces in tension and compression was both considered as $\phi A_s F_y$, with $\phi = 0.9$ and $F_y = 250$ MPa, where A_s is the cross section of the brace element (Sahoo and Chao, 2010).

According to the AISC's Seismic Provisions for Structural Steel Buildings (AISC, 2010), columns in BRB frames need to be checked for: first, the axial load and moment interaction for code level forces and second, the axial load only corresponding to the sum of the vertical component of all BRB applied to the column along with tributary gravity loads. For the columns of assumed models, second criterion governed the design and produced larger demand/capacity ratios. The maximum expected compression forces from the brace are calculated as $R_y \omega \beta A_s F_y$, where $R_y = 1.1$ is the material over strength, $\omega = 1.25$ considers the strain-hardening effect and $\beta = 1.1$ is the compression over-strength factor (Jones and Zareian, 2013). To design the beams connected to the BRBs, the horizontal

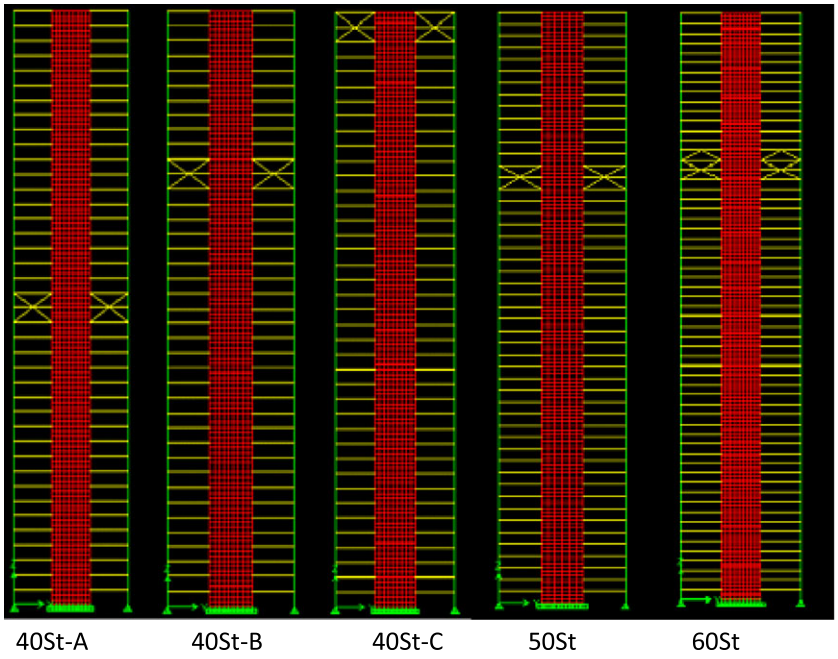

Figure 3. Elevation view of the structure models.

DOI: 10.1002/tal

component of the brace compression along with unbalanced upward component of the BRB was used (Sahoo and Chao, 2010). Table 1 shows the specification of the structures designed using the code prescriptive approach.

3. NONLINEAR MODELING

For assessment of the building behavior, the structures are modeled in PERFORM-3D software (PERFORM-3D, 2011). The columns and beams are modeled with elastic members. After each analysis, the elastic behavior of these elements is checked through controlling the demand/capacity ratio. The mass property is assigned to each floor at the center of mass, and rigid diaphragm is considered for the structure.

3.1. BRB modeling

BRB component of PERFORM-3D is a bar-type element that resists axial force only and has no resistance to torsional or bending forces (PERFORM-3D, 2006). The element consists of two bars in series. There is a linear portion incapable of yielding and a nonlinear portion capable of yielding.

The length of restrained nonlinear portion of a BRB element was assumed to be 0.7 of the node-to-node brace element length. The remaining 30% was considered as the linear portion that is the nonyielding portion. This linear portion of the brace accounts for the stiffness of the gusset, the brace connection and the portion of the column that is not considered in centerline to centerline geometry. Generally, the linear portion consists of the transition and the end segment (Figure 4). To prevent yielding of the linear portion, the cross-section area of the transition and end segment of BRBs are taken larger than the restrained nonlinear portion. The cross-section area of transition and end segments (A_t and A_e) of the BRB elements were chosen as 1.6 and 2.2 times the cross-section area of the core cross section, respectively. Besides, the length of the transition and end segments were chosen as 0.06 and 0.24 times the total length of the bracing (Nguyen *et al*., 2010).

To calculate the cross-section area of the yielding core (A_c) of the BRB element, the following equation was used (Bosco and Marino, 2013):

$$\frac{L_c}{A_c} = \frac{L_w}{A_{eq}} - \frac{L_e}{A_e} - \frac{L_t}{A_t} \tag{1}$$

where L_c, L_t, L_e and L_w represent the lengths of the yielding core, transition segment end segment and the whole bracing, respectively; also, A_{eq} is the cross-section area of the equivalent bar calculated from the linear design procedure. Figure 5 shows backbone curve for the BRB element used in the nonlinear model (Simpson, Gumpertz, Heger, Inc, 2009).

Table 1. Specification of the structures designed using the code prescriptive approach.

	40St-A	40St-B	40St-C	50St	60St
Core-wall height (m)	140	140	140	175	210
Wall length (X direction) L_w (m)	10	10	10	12.5	15
Wall thickness (m)	0.5	0.5	0.5	0.75	1.15
Outrigger stories no.	20, 21	29, 30	39, 40	36, 37	44, 45, 46
Brace cross-section area (m^2)	0.0445	0.0430	0.0362	0.0748	0.1239
Total seismic weight of structure (t)	37 000	37 000	37 000	75 000	138 000
Axial load ratio of core-wall at base ($P/A_g f_c$)	0.155	0.155	0.155	0.18	0.197
Normalized height of outrigger (from base)	0.5	0.73	0.98	0.73	0.74
Design base shear (t)	2220	2150	2340	4480	8390
T1	4.04	4.42	5.1	5.66	6.64
T2	1.09	0.9	0.93	1.12	1.26
T3	0.38	0.4	0.39	0.47	0.5

DOI: 10.1002/tal

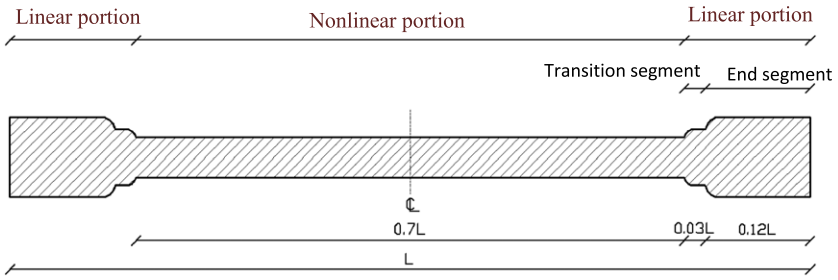

Figure 4. Schematic view of a BRB.

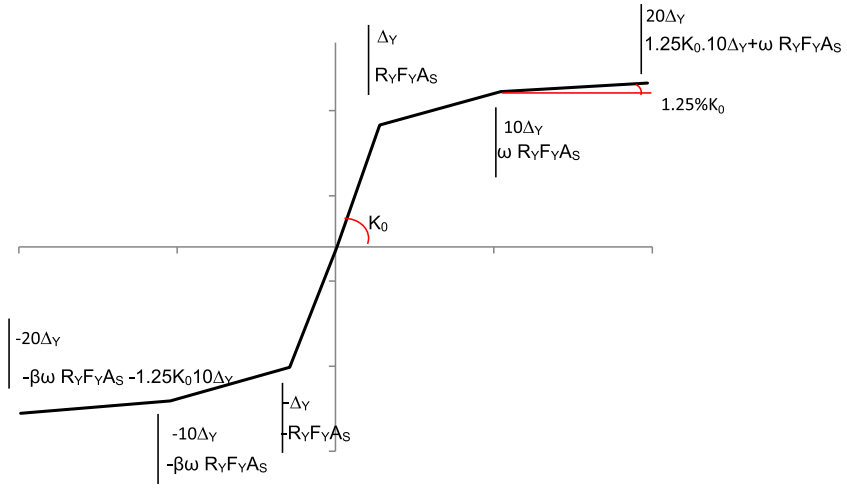

Figure 5. Backbone curve for the BRB element (Simpson, Gumpertz, Heger, Inc, 2009).

3.2. *Software verification*

Fiber models have preference over the lumped-plasticity beam–column models. Using the fiber element modeling, prediction of neutral axis migration within the RC concrete walls subjected to the lateral loads can be achieved (Applied Technology Council, 2010). Orakcal *et al.* and Beiraghi *et al.* have demonstrated the capability of the fiber element models to simulate the behavior of RC shear walls (Beiraghi *et al.*, 2015; Orakcal and Wallace, 2006).

In the wall elements, each element should have distinct longitudinal (vertical) and transverse directions: Axis 2 is the vertical one, axis 3 is the horizontal one, and axis 1 is normal to the plane of the element. For slender walls, it is sufficiently accurate to use one element per story (PERFORM-3D, 2006). Figure 6 shows how the shear wall elements could be used to model a 3D wall. Vertical in-plane behavior is usually more important than the transverse (horizontal) behavior. In the vertical direction, an element could be inelastic in bending and/or shear. Transverse in-plane behavior is assumed to be elastic and secondary. Out-of-plane bending is also secondary and is assumed to be elastic. As the fibers yield and/or crack in the inelastic fiber section, the effective centroid axis shifts (PERFORM-3D, 2006).

Experimental data from testing on a slender RC shear wall subjected to cyclic lateral loading was used to verify the accuracy of the model and to ensure correctness of the behavior of the shear wall elements (Thomsen and Wallace, 2004). Capacity design was used to design this specimen to allow for flexural hinging at its base. For modeling, five nonlinear shear wall elements over the height and eight concrete fibers plus eight steel fibers in each element were used (Figure 7). Inelastic strain tends to concentrate on a single element; therefore, an element length equal to the assumed plastic hinge length of $0.5L_w$ was used, where L_w is the core-wall length (ASCE/SEI 41-06, 2007). The lateral load versus top displacement relation is relatively insensitive to the mesh size and the number of material

DOI: 10.1002/tal

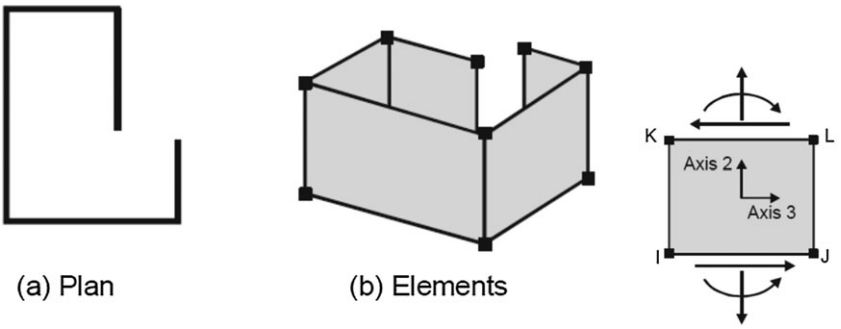

Figure 6. Shear wall element (PERFORM-3D, 2006).

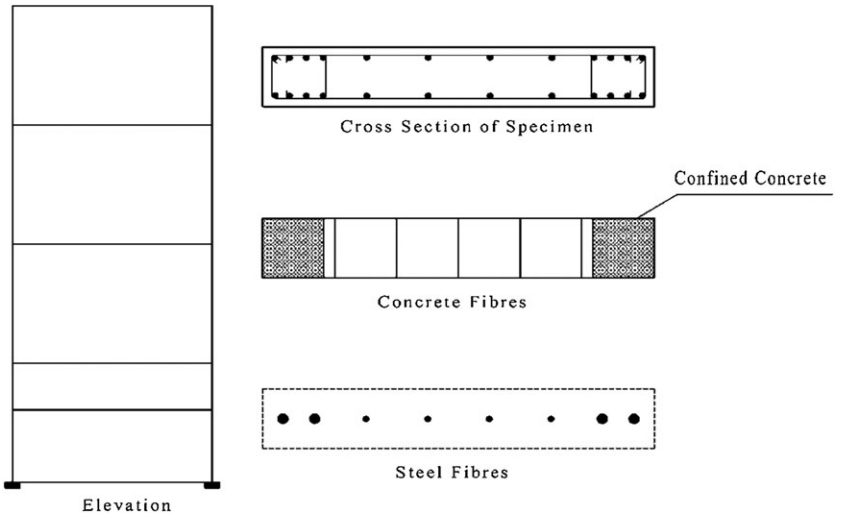

Figure 7. Fiber element model of the test wall.

fibers (Orakcal and Wallace, 2006). An axial force of $0.07A_g f_c$, where A_g is the area of the wall cross section and f_c is the concrete compression strength resulting from the test, is applied to the specimen and held constant throughout the test duration, and cyclic lateral displacement is applied at the top of the wall. Figure 8 compares the results of numerical and experimental hysteresis loops. The horizontal axis is the lateral drift at the top of the specimen.

3.3. Core-wall modeling

Shear wall elements are used to model RC walls. Each fiber cross section is comprised of the vertical steel and concrete fibers. For nonlinear fiber element, a model of confined concrete stress–strain based on the modified Mander model was assumed (Mander *et al*., 1988). Tensile strength of the concrete is ignored. The expected concrete compressive strength was 1.3 times the specified strength used for the design, and the expected yield strength of the steel reinforcement was 1.17 times its nominal yield strength (LATBSDC, 2011). The expected stress–strain graph of reinforcement and concrete is shown in Figure 9. Strength and stiffness degradation are applied through specifying the degradation factor for longitudinal reinforcements. This factor represents the ratio of the areas of the degraded to nondegraded hysteresis loops (Ghodsi *et al*., 2010). One element per story was used to model the core-wall (PERFORM-3D, 2006). Figure 10 shows the perspective view of the fiber element models.

Linear shear model was assumed in the models. A simple rule for selecting effective shear stiffness does not exist, and different references recommend varying effective shear stiffness. A typical value is $G_c A_g/10$ to $G_c A_g/20$ as recommended by ATC72 (Applied Technology Council, 2010). In the current research, $G_c A_g/15$ was used, where $G_c A_g$ was the elastic shear stiffness.

DOI: 10.1002/tal

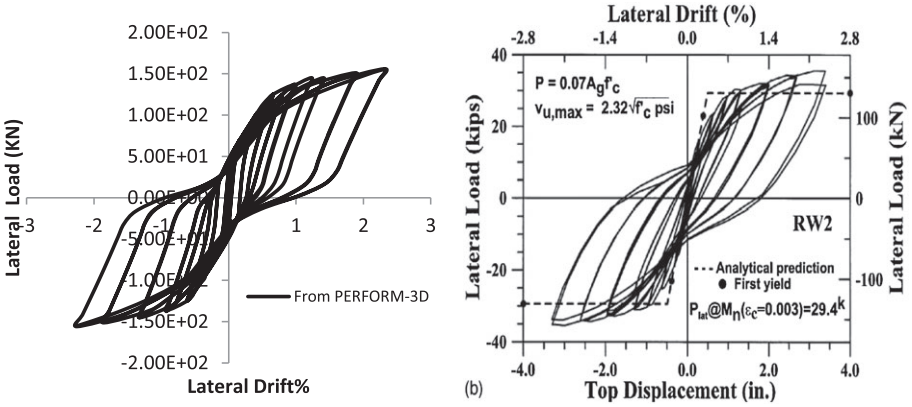

a) Numerical result b) Experimental result (Orakcal and Wallace, 2006)

Figure 8. Comparison of hysteresis loops from (a) numerical and (b) experimental results.

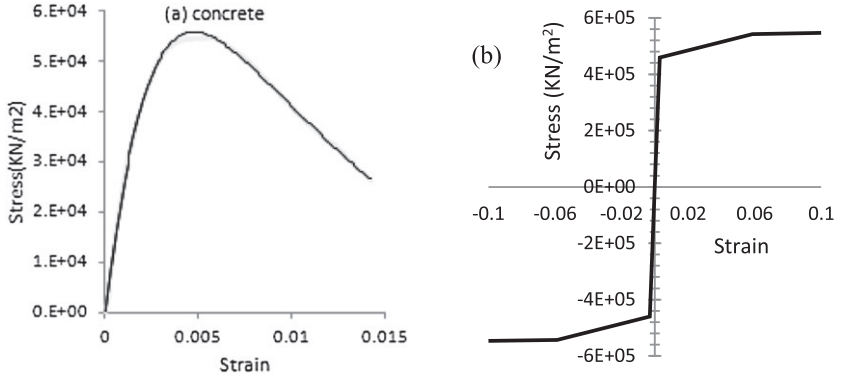

Figure 9. Stress–strain graph of (a) compression concrete and (b) reinforcement bar.

3.4. Damping consideration

Inappropriate damping assumptions may result in extravagantly unrealistic responses that considerably differ from the real responses of the buildings (Léger and Dussault, 1992). Chopra (2001) believes that Rayleigh damping can only be used when proper damping mechanisms are provided throughout the structure (Chopra, 2001).

PERFORM-3D software has the ability to implement Rayleigh damping as well as modal damping. The software user guide recommends use of a combination of modal and Rayleigh damping (PERFORM-3D, 2006). In this approach, a small amount of Rayleigh damping in addition to modal damping was used to damp out high-frequency vibrations. To use the Rayleigh damping, two modes should be selected. It is common to select the first mode and the mode for which the accumulated modal mass participation is >90% of the total mass. For this study, 2.5% of the modal damping for all modes along with 0.1% Rayleigh damping for the first and third modes was used according to the software guideline (PERFORM-3D, 2006).

3.5. Earthquake records

A set of 14 fare-fault earthquake records was used in the nonlinear time history analysis (NLTHA). They are represented in the Table 2. The scaling procedure described in the ASCE 7 was used to obtain the appropriate records at maximum considered earthquake level as illustrated in Figure 1. The scaling was over periods ranging from $0.2T$ to $1.5T$, where T is the estimated building period (ASCE/SEI 7-2010, 2010).

DOI: 10.1002/tal

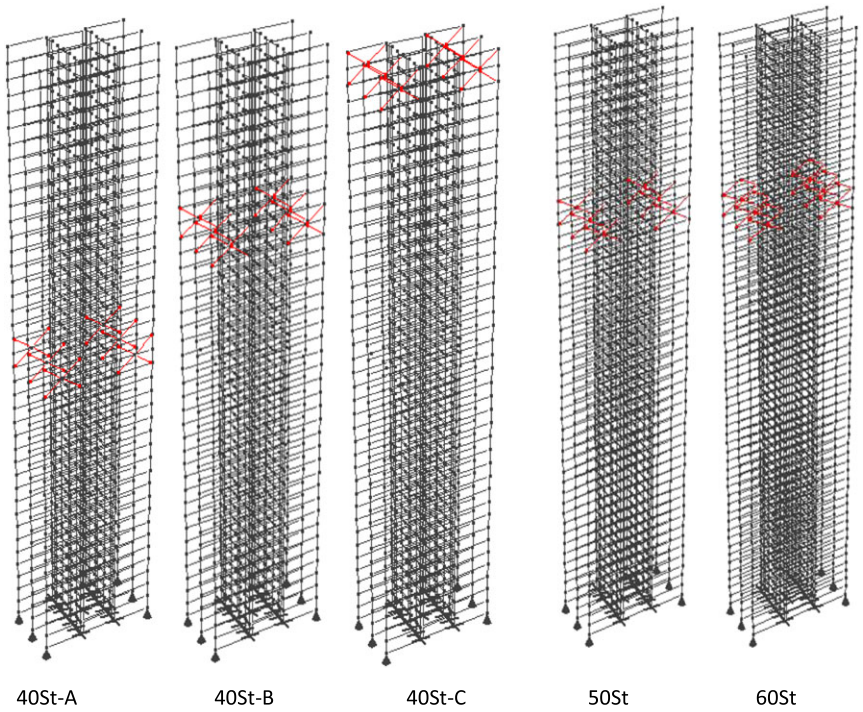

Figure 10. Perspective of the fiber element models.

4. RESPONSES FROM NONLINEAR TIME HISTORY ANALYSIS

Figure 11 shows the responses of the 40-story building, while the outrigger is placed at 0.5H, 0.73H and 0.98H. The reinforcement ratio obtained from the conventional RSA procedure was implemented in the NLTHA. Curvature ductility demand indicates the extension of plasticity in the RC core-walls. Figure 11(a) shows the average of the core-wall curvature ductility envelope over the height of the 40-story structure. The height of the building was normalized through dividing by the total building height. It is obvious that when the outrigger is placed at 0.5H, the curvature ductility demand, in the region above the outrigger level, reaches values approximately larger than those of the base curvature ductility demand, and plasticity is thoroughly extended to the upper levels of the RC core-wall region above the outrigger. This behavior is not expected by the designer in the conventional design procedure. Also, the curvature ductility demand at the base is a moderate value. The reason for this jump in the graph is curtailment of the longitudinal reinforcement, and the jumps are more intense above the outrigger. Besides, at the adjacent level below the outrigger level, the curvature ductility demand graph shows a rising.

If the outrigger is placed at 0.73H, the curvature ductility demand of the core-wall at the base and above the outrigger, as well as at the adjacent level below the outrigger, is increased compared with when the outrigger is located at 0.5H. Again, jump in the curvature ductility happens at levels where the reinforcement ratio changes.

If the outrigger is placed at the top level (adjacent to the roof), the plasticity extends adjacent to below of the outrigger as well as at the mid-height of the core-wall. The authors realized that this issue is more critical for 50-story and 60-story buildings with the outrigger at the top level. This issue has not been studied in this paper. Furthermore, maintaining mid-height levels in the elastic region requires excessive longitudinal reinforcement. Therefore, top level is not the preferred level for the outrigger.

Figure 11(b) shows the average of moment demand envelopes along the core-wall. The moment value has been normalized through dividing by the total seismic weight multiplied by the total height of the building (W.H). Generally, if the outrigger is placed at the higher level, the base moment demand increases slightly; if the outrigger is placed at the top level, a large amount of moment is exerted on the core-wall at this level. The reason is the longitudinal reinforcement ratio calculated from

DOI: 10.1002/tal

Table 2. Earthquake records used in the NLTHA.

Event name	Year	Record length (s)	Station	PGA	PGV	*M*	Site source distance (km)
Northridge	1994	20	Canyon Country-WLC	0.48	45	6.7	26.5
Duzce	1999	56	Bolu	0.82	0.62	7.1	41.3
Hector Mine	1999	45.3	Hector	0.34	42	7.1	26.5
Imperial valley	1979	100	Delta	0.35	33	6.5	33.7
Imperial valley	1979	39	El Centro Array#11	0.38	42	6.5	29.4
Kobe, Japan	1995	41	Shin-Osaka	0.24	38	6.9	46
Kocaeli, Turkey	1999	27.2	Duzce	0.36	59	7.5	98.2
Kocaeli, Turkey	1999	30	Arcelik	0.22	40	7.5	53.7
Landers	1992	44	Yermo Fire Station	0.24	52	7.3	86
Loma Prieta	1989	40	Gilroy Array	0.56	45	6.9	31.4
Superstition Hills	1987	40	El Centro lmp. Co.	0.36	46	6.5	35.8
Superstition Hills	1987	22.3	Poe Road (temp)	0.45	36	6.5	11.2
Chi chi, Taiwan	1999	90	Chy101	0.44	115	7.6	32
San Fernando	1971	28	LA-Hollywood Stor	0.21	19	6.6	39.5

PGA, peak ground acceleration; PGV, peak ground velocity.

the conventional RSA and used in the NLTHA. From this point of view, it seems that the top level is not a good position to locate the outrigger. When the outrigger is placed at 0.5H, the average moment demand, adjacent to below of the outrigger, is less than the moment demand adjacent to above of the outrigger. In the case that the outrigger is placed at 0.73H, this issue is vice versa. The reason is that if the outrigger is placed at 0.73H, the plastic moment strength of the wall adjacent to above of the outrigger is approximately 0.011W.H and the plastic moment strength in the core-wall underneath the outrigger is approximately 0.016W.H. Therefore, in the 40St-B approach, the moment demand envelope of the core-wall adjacent to underneath the outriggers is larger than the moment demand adjacent to above of the outrigger. In this case, the maximum moment exerted from the BRB outriggers is approximately 0.007W.H. It is worth to note that in the 40St-B approach, the vertical reinforcement ratio in the core-wall adjacent to underneath the outrigger is larger than the reinforcement ratio adjacent to above the outrigger (Table 5). This issue leads to a larger moment demand in the area adjacent to underneath the outrigger. This issue is reversed when the outrigger is placed at 0.5H. In the 40St-A approach, the value of plastic moment adjacent to underneath the outrigger is smaller than the one adjacent to above of outrigger. In all of the models, the BRBs exceed the linear elastic limit when subjected to each of the examined earthquake records.

Figure 11(c) presents the normalized shear envelope over the normalized height of the core-wall. The shear value has been divided by the seismic weight. Generally, there is a considerable shear slip in the shear diagram at the outrigger level. The base shear demand does not depend on the placement level of the outrigger. The reason is that the acceleration spectrum value for the considered 40-story tall building, with high period, is almost identical. Furthermore, the shear demand envelop adjacent to below the outrigger, especially when the outrigger is placed at the top level, shows swelling. This phenomenon corresponds to the higher modes effects of vibration.

Figure 11(d) shows the average of inter-story drift ratio (IDR) envelope for the 40-story core-wall with outrigger at different levels. It is obvious that if the outrigger is placed at 0.5H, the maximum IDR demand has considerably large value that is near 4%. It should be noted that the LATBSC states that the maximum allowable IDR for the average of responses is 3% (LATBSDC, 2011). Therefore, placement of the outrigger at 0.5H is not an appropriate decision. Moreover, Figure 11(d) demonstrates that if the outrigger is placed at 0.98H, the pattern of the IDR demand changes significantly.

Figure 11(e) shows the average of lateral displacement demand envelope for the 40-story building with outriggers at different positions. The displacement has been normalized through dividing by the total height of the building. In case of placing the outrigger at 0.5H, the lower half of the core-wall has less lateral displacement compared with the case of placing the outrigger at the 0.73H. If the outrigger is placed at 0.5H, the roof displacement demand would be 1.2 times the roof displacement demand obtained from placing the outrigger at 0.73H. The reason for this is the extreme plasticity extension in the core-wall above the outrigger that leads to larger displacement demand in the upper

DOI: 10.1002/tal

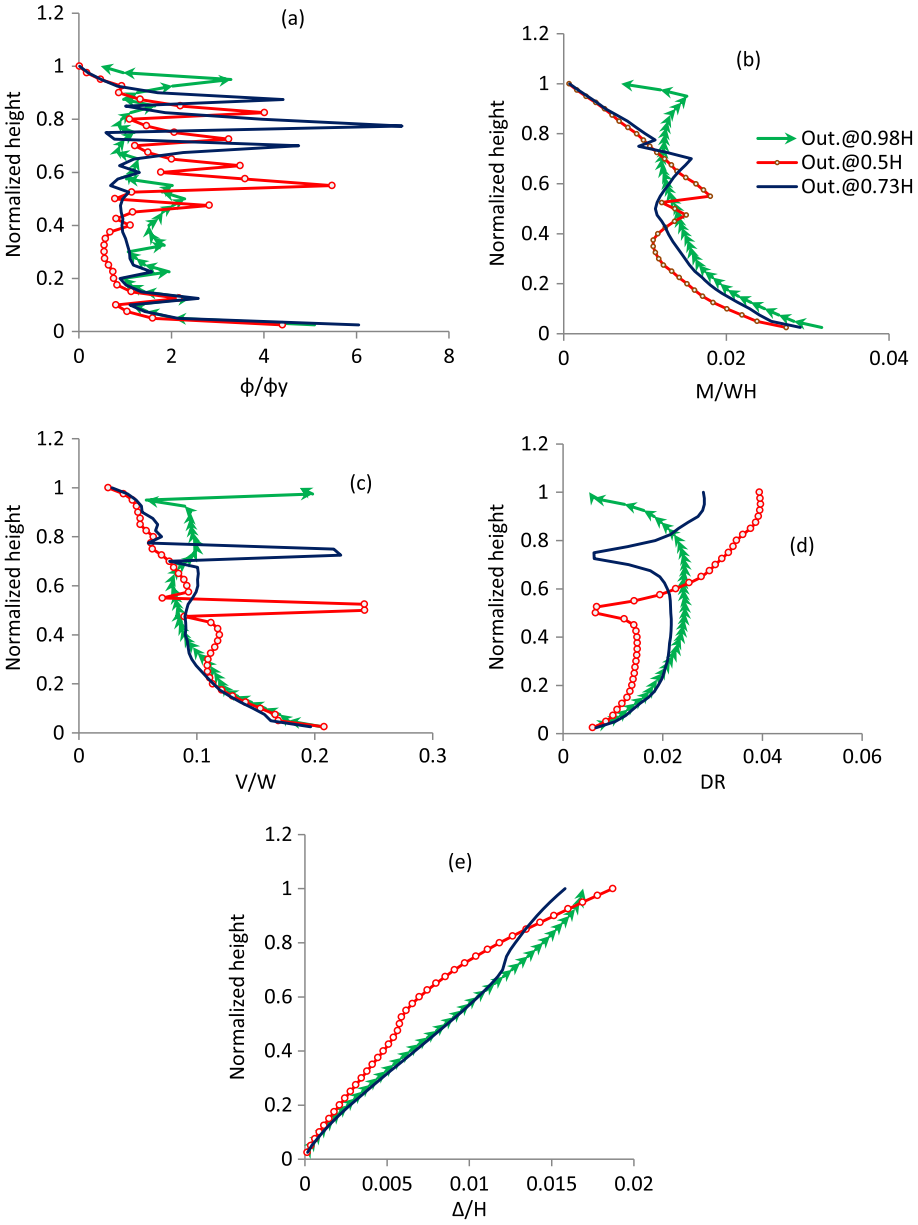

Figure 11. Average of the (a) curvature ductility, (b) moment, (c) shear, (d) inter-story drift ratio and (e) lateral displacement envelop, in 40-story core-wall.

levels in the first case. Therefore, placement of the outrigger at 0.5H is not recommended according to the displacement demand.

5. CAPACITY DESIGN APPROACH

The philosophy of capacity design in structural seismic engineering ensures that during an earthquake, the structure responds in a favorable ductile manner. This is achieved by pre-selecting an appropriate plastic mechanism and then providing special detailing to the plastic hinge regions. Providing enough ductility in these regions leads to energy dissipation under severe earthquakes (Park and Paulay, 1975; Paulay and Priestley, 1992). Capacity design approach can keep the large portion of the core-walls elastic and facilitate the detailing of the reinforcement there. The ease of detailing and reduction in

DOI: 10.1002/tal

the reinforcement along a significant portion of the core-wall are the advantages of capacity design. The performance of the structure should be controlled by plastic hinge formation.

According to the investigation in the previous section and considering the responses obtained from placing of the outrigger at three different levels of the 40-story building, the selected outrigger level for further investigation is 0.73H. It is obvious that 0.5H is not a suitable level for BRB outrigger because of very large IDR demand in the upper regions. For the outrigger at 0.98H, the moment envelope is the largest one along the lower half of the height; the reason is the large reinforcement calculated from RSA procedure. Besides, the moment and shear demand in the upper region, near the outrigger, are large values, and generally, large reinforcement quantity is required for the RC core-wall compared with the case of placing the outrigger at the 0.73H. Table 5 lists the vertical reinforcement ratio for the RC core-wall at the base and adjacent to the outrigger level for the 40-story building. For 40St-C approach, the reinforcement ratio in region just below the outrigger is near the reinforcement ratio at the base. The overall longitudinal reinforcement obtained from RSA approach in this case is approximately near twice the overall longitudinal reinforcement in 40St-B approach. It is worth to note that other researchers and specialists who studied outrigger systems with energy dissipation capability have not used these kinds of outrigger at the top level (Chen *et al*., 2010; Smith and Willford, 2007; Zhou and Li, 2013).

6. PROPOSED PROCEDURE

In this section, it is assumed that the outrigger is placed at 0.73H. If an identical R value is used to reduce responses of all the vibrational modes for design of the outrigger-core-walls during strong earthquake, the plasticity extension occurs anywhere over the height. Therefore, conventional RSA is not appropriate for designing outrigger–core-wall systems. One solution is to reduce the flexural responses of different vibrational modes using different response modification factors. The aim of this section is to find new R factors for each modal response in the design procedure.

Generally, there is a considerable curvature ductility demand in the core-wall adjacent to the outrigger level. Therefore, in an outrigger–core-wall structure, three regions within the core-wall show relatively large moment demand. These are the regions close to the base, adjacent to below and above the outrigger. According to the author's investigation, it is preferred to allow these regions for plasticity extension because restraining these regions in the elastic range, during the strong earthquake, is a difficult and expensive issue. In the region below and above the outrigger level, restricting the RC core-wall in the elastic range requires using large quantity of vertical reinforcement around 3.5%, even larger than twice the base reinforcement ratio. At the upper levels and near the outrigger, it is not easy to restrain the plasticity extension in the core-wall. One reason is the small value of axial compression on the core-wall in upper regions. Besides, considering the curvature ductility demand of the core-walls, it could be understood that formation of three plastic hinges within the outrigger-core-walls is preferred. This approach is called the triple-plastic hinge. Figure 12(a, b) shows the schematic

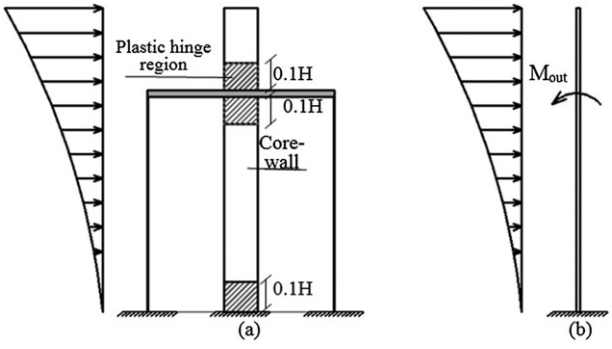

Figure 12. (a) Schematic elevation of three plastic hinge concepts in the RC core-wall and (b) moment exerted from outrigger on the core-wall.

DOI: 10.1002/tal

representation of the triple-plastic hinge approach in the outrigger–core-wall system and moment exerted on the core-wall at outrigger level. To reach a balanced curvature ductility demand in the three predefined plastic hinge regions within the core-walls subjected to strong earthquakes, an appropriate design moment value should be taken for the system. A trial and error process was applied to obtain the appropriate R coefficients to reduce elastic moment demand of different vibration modes. The suitable R factors should lead to appropriate curvature ductility demand in the plastic hinge regions in the nonlinear dynamic analysis. In this approach, the effect of the first four elastic modes of vibration was reduced by different R factors. In each case, the vertical reinforcement ratio in the plastic hinge regions was designed for corresponding moment demand. Considering the capacity design method, the plasticity should not extend in the outside of the specific plastic hinge regions. Thus, in the outside of the plastic hinge region, the reinforcement ratio must be calculated by using an amplified moment demand. By using the new calculated reinforcement ratios in the corresponding areas throughout the core-wall model, NLTHA was implemented for the system. Then, the curvature ductility envelope was examined. If the curvature ductility values in the three plastic regions were not balanced, the work would be repeated for another R factors. Finally, the following combination was proposed:

$$M^2 = \left(\frac{M_{ERS1}}{3.8}\right)^2 + \left(\frac{M_{ERS2}}{3.5}\right)^2 + \left(\frac{M_{ERS3}}{2}\right)^2 + \left(\frac{M_{ERS4}}{1}\right)^2 \tag{2}$$

where M is the design moment demand of the plastic hinge regions and M_{ERSi} is the ith modal moment demand. It is obvious that the R factor for the first, second, third and fourth modes is 3.8, 3.5, 2 and 1, respectively. It appears that the effects of the higher mode of vibration do not reduce considerably by the plasticity extension in the plastic regions. It is worth to notice that the proposed R factors are certainly valid for the considered 40-story, 50-story and 60-story core-wall buildings, and more research needs to investigate the accuracy of the proposed R factors for other RC core-wall buildings with BRB outriggers. Therefore, it seems that all the results and responses presented in this study are reasonable for the mentioned structures.

To ensure that the plasticity does not extend in the region outside the considered plastic hinge within the core-wall, a capacity design concept should be implemented. To fulfill this purpose, the bending moment strength of the region located outside the hinge area should be enough. Therefore, the design moment diagram between the base plastic hinge area and the plastic hinge adjacent to below the outrigger, both obtained from Eq. (2), should be amplified. To calculate this amplification factor, the following equation is used to calculate the over strength factor at the top of the base plastic hinge.

$$\Phi_0 = \frac{M_{pr}}{M_u} \tag{3}$$

where M_{pr} is the probable flexural strength of the core-wall in plastic hinge region, determined using the expected yield strength of the steel reinforcement and incorporating a strength reduction factor of 1 and M_{u} is the factored moment in the level just above the plastic hinge region. The portion of moment diagram between the base plastic hinge and the hinge below the outrigger, calculated from Eq. (2), is amplified by the Φ_0 corresponding to the base hinge ($\Phi_{0\mathrm{b}}$). Besides, the portion of moment demand curve above the highest plastic hinge, adjacent to above the outrigger, is amplified by the corresponding Φ_0 of that plastic hinge ($\Phi_{0\mathrm{up}}$) (Table 3).

The design moment diagram along the height obtained from the conventional RSA and from the proposed procedure is presented in Figure 13 for the 40-story, 50-story and 60-story buildings. Generally, in the proposed procedure, the design moment at the base is reduced compared with the conventional procedure, and this issue is reverse at upper levels.

DOI: 10.1002/tal

Table 3. Moment amplification factor in the proposed procedure.

	Φ_{0b}	Φ_{0up}
40St	1.51	1.3
50St	1.42	1.27
60St	1.32	1.25

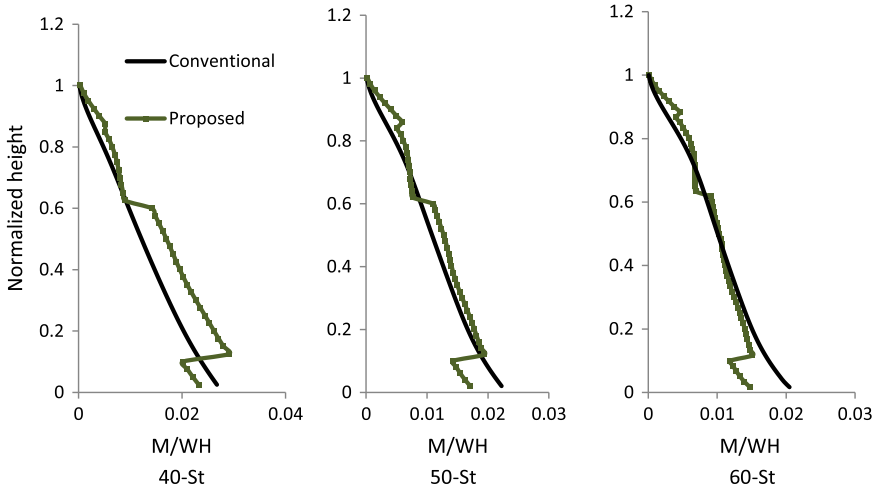

Figure 13. The design moment diagram obtained from conventional RSA and from the proposed formula.

7. RESPONSES FROM PROPOSED PROCEDURE

The 40-story, 50-story and 60-story buildings are designed using both proposed procedure and conventional RSA procedure prescribed in the codes. To design the BRBs in all the cases, a response modification factor equal to 5 was used according to the conventional procedure. The mean of the maximum strain divided by the yielding strain in the BRB cores, obtained from the dynamic analysis, has been shown in Table 4. The average of maximum strain in the BRBs obtained using both the conventional and proposed design approaches was less than 10 times the yielding strain that is within the acceptable limit (Jones and Zareian, 2013).

The core-wall longitudinal reinforcement ratios at three plastic hinge regions, calculated from the two aforementioned approaches, have been presented in Table 5. NLTHA of the models has been implemented for comparison of the responses.

Figure 14 compares the curvature ductility demand obtained from the conventional and proposed procedures. It is obvious that for the 60-story building, using conventional procedure leads to a small curvature ductility demand equal to 2 at the base level of the core-wall and also undesirable rise of curvature ductility in the region above the base plastic hinge, as well as around 0.85H. These imperfections have been removed using the proposed design procedure; for example, curvature ductility demand at the base has been increased at the base region. The general curvature ductility demand envelops from conventional procedures in the 40-story and 50-story core-walls are almost

Table 4. Average of max strain to yielding strain in the BRB core.

	Max strain/yielding strain	
Procedure	Conventional	Proposed
40St	9.2	9.6
50St	6.5	6.8
60St	4.5	5.2

DOI: 10.1002/tal

Table 5. Longitudinal reinforcement obtained from conventional and proposed procedure.

		40St-A	40St-B	40St-C	50St	60St
Reinforcing ratio at base	Conventional	1.03	1.27	1.64	1.48	1.72
	Proposed procedure	—	0.85	—	0.53	0.25
Reinforcing ratio at adjacent below the outrigger	Conventional	0.46	0.9	1.51	0.75	0.57
	Proposed procedure	—	0.92	—	0.79	0.49
Reinforcing ratio at adjacent above the outrigger	Conventional	1.15	0.62	—	0.68	0.52
	Proposed procedure	—	0.87	—	0.86	0.73

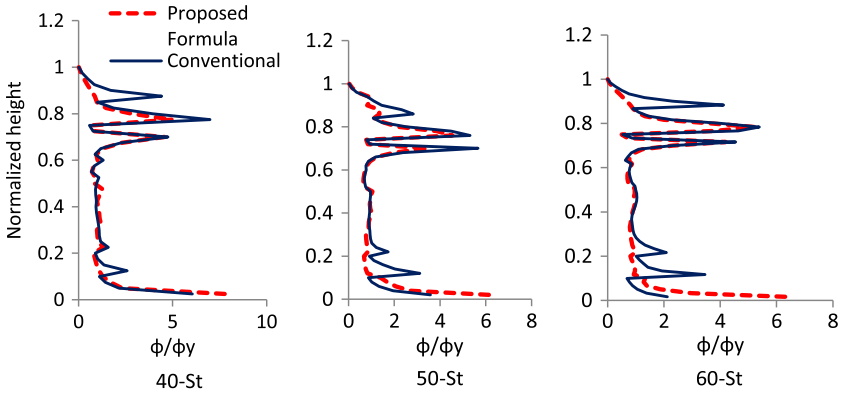

Figure 14. Comparing the curvature ductility demand obtained from conventional and proposed procedures.

similar to the graph of 60-story building. However, for the taller outrigger structure in the conventional procedure, the curvature ductility demand is smaller at the base of the core-wall. Also, Figure 14 demonstrates that the proposed procedure causes balanced curvature ductility demands within the distinct plastic hinge regions and prevents plasticity extension in the other regions.

Figure 15 demonstrates that the moment demand envelope of the RC core is affected by the proposed approach. In the 40-story building, the largest difference between the conventional and proposed approach is less than 15%. The proposed approach leads to lower amounts of reinforcement and less moment demand at the base. But, concerning the upper levels, this issue is vice versa because the main purpose is to control ductility demand. For the 60-story building, the moment demand obtained from the proposed approach is 0.75 times the moment demand obtained from the conventional approach; the reason is the reduction of moment strength in the core-wall base region in the new approach.

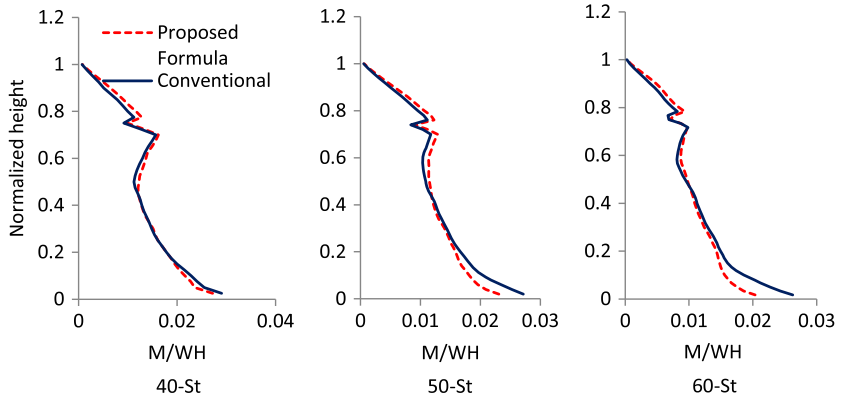

Figure 15. Comparing the moment demand obtained from conventional and proposed procedures.

DOI: 10.1002/tal

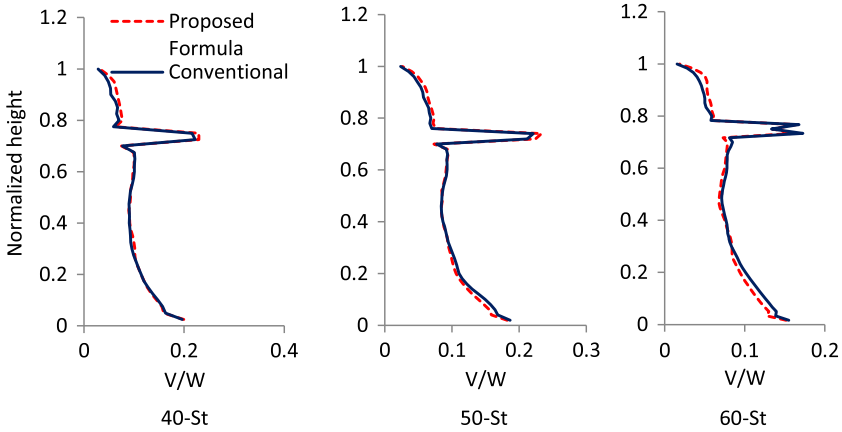

Figure 16. Comparing the shear demand obtained from conventional and proposed procedures.

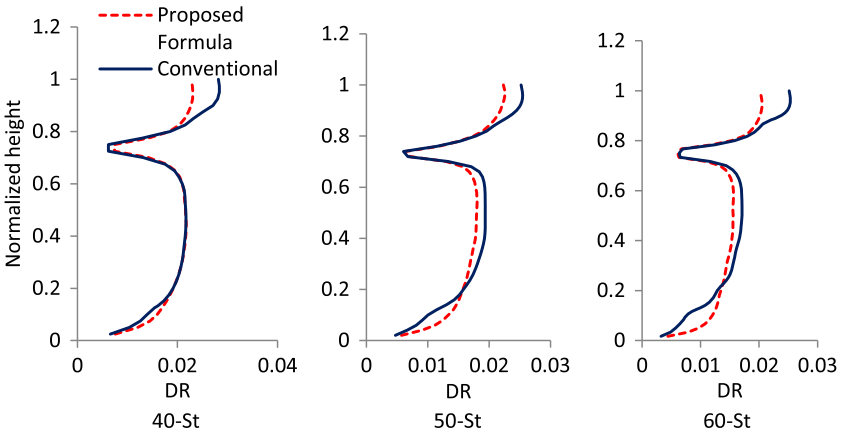

Figure 17. Comparing the inter-story drift ratio demand obtained from conventional and proposed procedures.

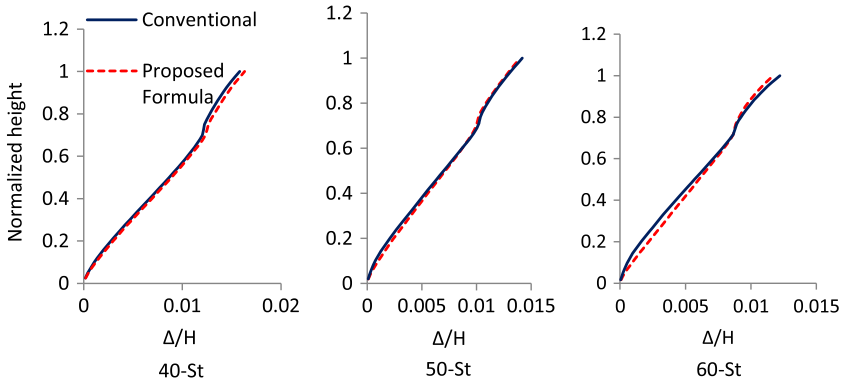

Figure 18. Comparing the lateral displacement demand obtained from conventional and proposed procedures.

Figure 16 shows the normalized shear demand envelope of the core-walls over the height obtained from the conventional and proposed design procedures. For each considered height of the models, it is obvious that the shear demand envelopes calculated from the two procedures are nearly identical. Concerning the outrigger–core-wall structures, the shear demand envelope does not depend on the plastic hinges arrangement.

DOI: 10.1002/tal

Figure 17 shows the IDR demand envelopes of the core-walls over the structure height. In the 60-story building, the proposed procedure leads to about 20% reduction in the maximum IDR. For the 40-story and 50-story buildings, the reduction ratios are 20 and 10% respectively. The reason for this is that in the conventional procedure, plasticity extends anywhere over the height. While in the proposed procedure, plasticity is concentrated on the predefined locations. This evidence confirms the capability of the proposed design procedure.

Figure 18 shows the normalized lateral displacement demand envelopes obtained from the proposed and conventional procedures. Generally, the roof drift demand from the two procedures is identical. This issue demonstrates equal displacement rule for the tall buildings with high periods.

8. CONCLUSIONS

BRB outriggers can cause changes in the responses, like the force distribution and lateral displacement demand of the core-wall buildings. Therefore, formation of other plastic hinges within the RC core-wall, in addition to the one plastic hinge at the base, is probable. In this paper, core-wall buildings with BRB outriggers were designed using the conventional RSA. The outrigger was placed at 0.5H, 0.73H and 0.98H. The responses of these buildings were investigated using the NLTHA. It was demonstrated that placing outrigger at 0.73H leads to the more acceptable responses. Using the conventional design approach, it was showed that the plasticity extends anywhere within the core-wall, specially, at the region above the outrigger. Besides, the curvature ductility demand in the upper region is larger than that of the base. To reach desirable responses, a new modal combination method was proposed for design of these structures. In the proposed approach, different values of response modification factor were used for different modes to obtain the design moment of the core-wall plastic hinges. Three plastic hinge regions: at the base, adjacent to above and adjacent to below the outrigger level, were the preferable areas for the hinge formation. In the new approach, a capacity design concept was applied to prevent extension of plasticity outside of the plastic hinge regions. The results obtained from the NLTHA showed that the plasticity extended in the hinges and the curvature ductility demand of the three hinges had balanced values. Besides, the plasticity does not extend in other regions outside the hinge region of the core-wall buildings. The proposed approach leads to less moment demand at the base and less maximum IDR compared with the conventional approach. The base shear demand in the two approaches is almost identical. The average of maximum strain in the BRBs obtained by using both the conventional and proposed design approaches was within the acceptable limit.

ACKNOWLEDGEMENTS

This paper is the result of a research project in Islamic Azad University, Mahdishahr Branchand the authors would like to thank Islamic Azad University, Mahdishahr Branch, for the financial support.

REFERENCES

ACI 318-11. 2011. Building code requirements for structural concrete and commentary. ACI Committee 318: Farmington Hills.

AISC. 2010. Seismic provision for structural steel buildings. American Institute of Steel Construction: Chicago; 2005.

Applied Technology Council. 2010. ATC-72: Modeling and Acceptance Criteria for Seismic Design and Analysis of Tall Buildings. ATC: Redwood City, CA.

Asgarian B, Shokrgozar HR. 2009. BRBF response modification factor. *Journal of Constructional Steel Research* **65**: 290–298.

ASCE/SEI 7-2010. 2010. Minimum design loads for buildings and other structures. American Society of Civil Engineers: Reston, VA.

ASCE/SEI 41-06. 2007. Seismic rehabilitation of existing buildings (Including Supplement # 1). American Society of Civil Engineers: Reston, VA.

Beiraghi H, Kheyroddin A, Kafi MA. 2015. Nonlinear fiber element analysis of a reinforced concrete shear wall subjected to earthquake records. *Transactions of Civil Engineering* **39**(C2+): 409–422.

Beiraghi H, Kheyroddin A, Kafi MA. 2016a. Forward directivity near-fault and far-fault ground motion effects on the behavior of reinforced concrete wall tall buildings with one and more plastic hinges. *The Structural Design of Tall and Special Buildings* **25**(11): 519–539.

DOI: 10.1002/tal

Beiraghi H, Kheyroddin A, Kafi MA. 2016b. Energy dissipation of tall core-wall structures with multi-plastic hinges subjected to forward directivity near-fault and far-fault earthquakes. *The Structural Design of Tall and Special Buildings. Article first published online*. DOI:10.1002/tal.1270.

Beiraghi H, Kheyroddin A, Kafi MA. 2016. Effect of record scaling on the behavior of reinforced concrete core-wall buildings subjected to near-fault and far-fault earthquakes. *Scientia Iranica . article in press*.

Bosco M, Marino EM. 2013. Design method and behavior factor for steel frames with buckling restrained braces. *Earthquake Engineering & Structural Dynamics* **42**: 1243–1263. DOI:10.1002/eqe.2269.

Calugaru V, Panagiotou M. 2012. Response of tall cantilever wall buildings to strong pulse type seismic excitation. *Earthquake Engineering and Structural Dynamics* **41**: 1301–1318.

CEN EC8. 2004. Design of Structures for Earthquake Resistance. European Committee for Standardisation: Brussels, Belgium.

Chen Y, McFarland DM, Wang Z, Spencer BF, Bergman LA. 2010. Analysis of Tall Buildings with Damped Outriggers. *Journal Of Structural Engineering* **136**(11): 1435–1443.

Chopra AK. 2001. Dynamics of structures. Prentice-Hall: New Jersey.

CSA Standard A23.3-04. 2005. Design of Concrete Structures. Canadian Standard Association: Rexdale, Canada; 214.

ETABS, Version 13.1.1. 2013. Computers and Structures. Inc.: Berkeley, California, USA.

Ghodsi T, Ruiz JF, Massie C, Chen Y. 2010. Pacific earthquake engineering research/seismic safety commission tall building design case study. *The Structural Design of Tall and Special Buildings* **19**(2): 197–256.

Jones P, Zareian F. 2013. Seismic response of a 40-storey buckling-restrained braced frame designed for the Los Angeles region. *The Structural Design of Tall and Special Buildings* **22**(3): 291–299. DOI:10.1002/tal.687.

Kim J, Park J, Kim S. 2009. Seismic behavior factors of buckling restrained braced frames. *Structural Engineering and Mechanics* **33**(3): 261–284.

Klemencic R, Fry A, Hooper JD, Morgen BG. 2007. Performance based design of ductile concrete core wall buildings—issues to consider before detail analysis. *The Structural Design of Tall and Special Buildings* **16**: 599–614.

LATBSDC. 2011. An Alternative Procedure For Seismic Analysis and Design of Tall Buildings Located in the Los Angeles Region. Los Angeles Tall Buildings Structural Design Council: Los Angeles.

Léger P, Dussault S. 1992. Seismic-energy dissipation in MDOF structures. *Journal of Structural Engineering* **118**(5): 1251–1269.

Mahmoudi M, Zaree M. 2010. Evaluating response modification factors of concentrically braced steel frames. *Journal of Constructional Steel Research* **66**: 1196–1204.

Mander JB, Priestley MJN, Park R. 1988. Theoretical stress-strain model for confined concrete. *ASCE Journal of Structural Engineering* **114**(8): 1804–1826.

National Institute of Standards and Technology. 2012. Seismic design of cast-in-place concrete special structural walls and coupling beams, NEHRP Seismic Design Technical Brief No. 6 2012.

Nguyen AH, Chintanapakdee C, Hayashikawa T. 2010. Assessment of current nonlinear static procedures for seismic evaluation of BRBF buildings. *Journal of Constructional Steel Research* **66**(8–9): 1118–1127.

NZS 3101. 2006. New Zealand Standard, Part 1- The Design of Concrete Structures. Standards New Zealand: Wellington, New Zealand.

Orakcal K, Wallace JW. 2006. Flexural modeling of reinforced concrete walls-experimental verification. *ACI Structural Journal* **103**(2): 196–206.

Panagiotou M, Restrepo J. 2009. Dual-plastic hinge design concept for reducing higher-mode effects on high-rise cantilever wall buildings. *Earthquake Engineering and Structural Dynamics* **38**: 1359–1380.

Park R, Paulay T. 1975. Reinforced concrete structures. Wiley: New York, United States of America.

Paulay T, Priestley MJN. 1992. Seismic Design of Reinforced Concrete and Masonry. Wiley: New York, United States of America.

Priestley MJN, Calvi GM, Kowalsky MJ. 2007. Displacement-Based Seismic Design of Structures. IUSS Press: Pavia, Italy. ISBN:88-6198-000-6.

PERFORM-3D. 2006. Nonlinear Analysis and Performance Assessment for 3D Structures. V.4, User Guide. Computers and Structures, Inc.: Berkeley, CA.

PERFORM-3D. 2011. Nonlinear Analysis and Performance Assessment for 3D Structures, V.4.0.3. Computers and Structures, Inc.: Berkeley, CA.

Rahgozar R, Sharifi Y. 2009. An approximate analysis of framed tube, shear core and belt truss in high-rise building. *Structural Design of Tall and Special Buildings* **18**: 607–624.

Sahoo DR, Chao S. 2010. Performance-based plastic design method for buckling-restrained braced frames. *Engineering Structures* **32**: 2950–2958.

Satake N, Suda K, Arakawa T, Sasaki A, Tamura Y. 2003. Damping evaluation using full-scale data of buildings in Japan. *Jurnal of Structural Engineering* **129**(4): 470–477.

Simpson, Gumpertz, Heger, Inc. 2009. Detailed Design Writeup for BRBF building. Simpson, Gumpertz, & Heger, Inc.: San Francisco, CA.

Smith RJ, Willford MR. 2007. The damped outrigger concept for tall buildings. *Structural Design of Tall and Special Buildings* **16**(4): 501–517.

Smith BS, Coull A. 1991. Tall building Structures: Analysis and Design, 1 edn. John Wiley & Sons Inc.: New York.

Smith BS, Salim I. 1981. Parameter study of outrigger-braced tall building structures. *Journal of the Structural Division* **107**(10): 2001–2014.

Soong TT, Spencer BF. 2002. Supplemental energy dissipation: state-of-the-art and state-of-the-practice. *Engineering Structures* **24**(3): 243–259.

Taranath BS. 1974. Optimum belt truss location for high rise structures. *Engineering Journal*: 18–21.
Taranath BS. 1988. Structural Analysis and Design of Tall Buildings. Mc Graw Hill: New York.
Thomsen JH, Wallace JW. 2004. Experimental verification of displacement-based design procedures for slender reinforced concrete structural walls. *Journal of Structural Engineering, ASCE* **130**(4): 618–630.
Wu JR, Li QS. 2003. Structural performance of multi-outrigger-braced tall buildings. *The Structural Design of Tall and Special Buildings* **12**(2): 155–176.
Xu PF, Huang JF, Xiao CZ, Li YG, Huang SM. 1999. Some problems in seismic design of frame–core wall structures with strengthened stories. *Journal of Building Structures* **20**(4): 2–10.
Zhou Y, Li H. 2013. Analysis of a high-rise steel structure with viscous damped outriggers. *The Structural Design of Tall and Special Buildings* **23**(13): 963–979.

AUTHORS' BIOGRAPHIES

Hamid Beiraghi was born in 1979 in Sangesar, Iran. He obtained his BS degree in Civil Engineering from the Department of Civil Engineering at Sharif University of Technology, Iran, in 2000, his first MS degree in Construction Management and Engineering from Tehran University, in 2002, his second MS degree in Earthquake Engineering from International Institute of Earthquake Engineering and Seismology, Iran, in 2006, and his PhD degree in Structural Engineering from Semnan University, Iran, in 2015. His research focuses on the tall building response under near-fault pulse-like earthquakes and design of core-wall structures. He has published more than 20 journal and conference papers, and one book. He is a Faculty Member of Azad University, Mahdishahr Branch, Sangesar, Iran. He has also supervised numerous MS thesis.

Navid Siahpolo was born in 1982. He obtained his BS degree in Civil Engineering from the Department of Civil Engineering at Chamran university of Ahwaz, Iran, in 2003, and his MS degree from Persian-Gulf University, Bushehr, Iran, in 2006. Also He graduated from Semnan University in the field of Earthquake engineering with the. The subject of his Ph.D. dissertation is about the effect of near-fault pulse-like earthquakes on frame structures and development of practical equations for quick assessment and design of steel structures. He has published more than 30 journal and conference papers, and 2 books. He is now working as an assistant professor of the Civil Engineering department at Khuzestan ACECR Institute for Higher Education.

DOI: 10.1002/tal